High-Capacitance Organic Nanodielectrics: Effective Medium Models of Their Response

Sara A. DiBenedetto, Irina Paci, Antonio Facchetti, Tobin J. Marks,* and Mark A. Ratner*

Department of Chemistry and the Materials Research Center, Northwestern University, Evanston, Illinois 60208

Received: April 4, 2006; In Final Form: August 2, 2006

Molecular and macromolecular high-permittivity organic gate dielectric materials have been the focus of recent experimental research as a consequence of their promising properties for organic and inorganic field effect transistor (FET) applications. Two types of molecular thin films, self-assembled nanodielectrics (SANDs) and cross-linked polymer blends (CPBs), have been shown experimentally to afford high capacitances and low FET operating voltages. In an effort to design optimized nanostructures having even larger capacitances, lower leakage current densities, and further reduced FET operating voltages, we discuss approaches for computing the effective permittivities of each nanodielectric motif and investigate how molecular arrangements impact overall device capacitance. The calculated frequency-dependent capacitances, derived from Maxwell−Wagner theory applied to the Maxwell−Garnett effective medium approximation, agree fairly well with the experimental values for the two types of nanodielectrics. Predictions of larger capacitance SANDs are made with the two-capacitors-in-series equivalent circuit, where the layered, self-assembled structure is viewed as two different capacitors. The Maxwell−Garnett and Polder−Van Santen effective medium approximations are used to predict the dielectric response of higher permittivity polymer cross-linked blends. In calculations showing good agreement between theory and experiment, and with all parameters being equal, it is found that greater capacitances should be achievable with cross-linked composites than with layered composites.

I. Introduction

Thin films of polymeric materials, such as self-assembled monolayers,[1,2] self-assembled multilayers,[3] and cross-linked polymer blends,[4−6] have found applications as gate dielectrics in field effect transistors (FETs) fabricated with organic small molecules and polymers (OFETs),[3,4] single-wall carbon nanotubes,[7] ZnO nanowires,[8] and inorganic oxide thin films[9] as the channel semiconductor. When one of these organic nanodielectrics replaces conventional low-permittivity gate dielectrics such as SiO_2, FET device performance is greatly improved, exhibiting dramatically lower operating voltages and reduced current−voltage hysteresis.[10,11] These important results have directed research in the field of solid dielectrics to focus on the development of new materials with high permittivities and low leakage currents. With sufficient permittivities (∼20), organic thin film materials may also be useful in other high-capacitance applications such as pulsed-power capacitors.[12,13]

Solution-processable organic composites must have dielectric properties that are comparable to those of conventional materials, such as SiO_2, if they are to be used as a gate dielectric in OFETs (Figure 1a). In OFETs, the current between the source and drain electrodes is directly proportional to the gate voltage, the semiconductor mobility, and the capacitance per area (C) of the gate dielectric.[14] The capacitance for a thin film in a parallel plate capacitor (Figure 1b) is given by

$$C = \frac{\epsilon_0 \epsilon_r}{d} \tag{1}$$

where ϵ_r is the permittivity of the dielectric, ϵ_0 is vacuum permittivity (8.85×10^{-14} F/cm), and d is the thickness of the dielectric layer. Thus, the capacitance is increased by increasing the permittivity and/or by reducing the thickness. A typical OFET SiO_2 gate dielectric layer (permittivity of 3.9)[15] has a thickness in the 100−300 nm range and exhibits capacitance values in the 11−34 nF/cm^2 range. Using SiO_2 as the gate dielectric with a high-performance organic semiconductor, such as pentacene (having mobility in the 1.0 cm^2/(V s) range), yields OFET devices that operate in the 30−100 V range.[11,13] Lowering the operating voltage by reducing the SiO_2 thickness may appear to be the most straightforward solution; however, it is known that SiO_2 thicknesses below ∼3 nm frequently lead to detrimental FET gate leakage currents and increased device power consumption.[16,17] Since the SiO_2 dielectric thickness cannot be reduced further, increasing the permittivity is the only other realistic means to increase the parallel plate capacitance. In principle, self-assembled superlattices or polymer-based composites could be superior OFET gate dielectrics over traditional high-ϵ_r inorganic oxides because of their amenability to forming conformal, low-leakage, nanometer-thick insulating films by solution-based processes at low temperatures. Furthermore,

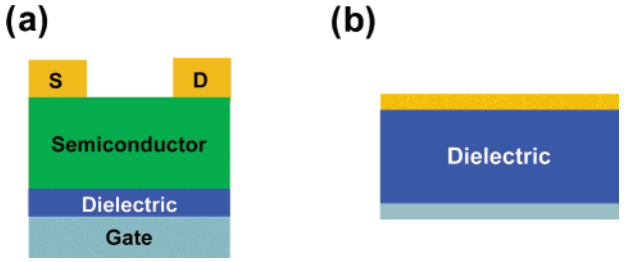

Figure 1. (a) Representative top-contact OFET device structure and (b) gate dielectric in a parallel plate capacitor structure.

* To whom correspondence should be addressed. E-mail: t-marks@northwestern.edu; ratner@chem.northwestern.edu.

10.1021/jp062096a CCC: $33.50
Published on Web 10/17/2006

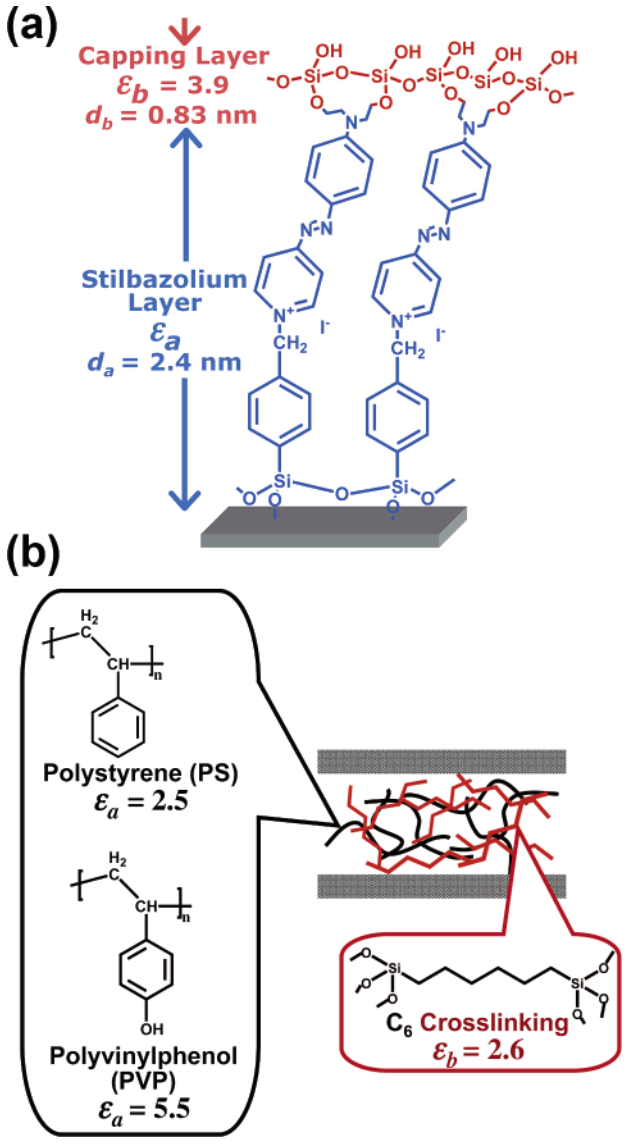

Figure 2. (a) Chemical structures and metrical parameters of the SAND nanodielectric.[3] (b) Chemical structures and metrical parameters of the CPB nanodielectric.[4]

because of their tailorable structures, their permittivities could potentially exceed that of SiO_2 or other oxide dielectrics.[11,18]

In an effort to optimize organic dielectric capacitances, we focus here on strategies to predict the permittivities of the self-assembled and cross-linked polymeric thin films, sketched in Figure 2, using established effective medium approximations.[19−24] We seek to understand how the permittivities and the molecular arrangements of the components impact their capacitance and, ultimately, their effectiveness as gate dielectrics in OFETs.

The self-assembled nanodielectric (SAND) has a multilayer composite structure (Figure 2a), which is fabricated via a layer-by-layer solution-phase self-assembly procedure using silane precursors.[3] The electrical and capacitance properties of this nanodielectric were characterized in a metal−insulator−metal (MIM) device configuration (indium-tin-oxide/insulator/Au). The SAND structure was found to be pinhole-free and to have excellent insulating properties: the MIM device measured capacitance as high as 2500 nF/cm^2 and leakage current densities as low as 10^{-8} A/cm^2. It was concluded that this self-assembly method should be extendable to other high-permittivity π-electron molecules, offering higher capacitance nanodielectrics.[3] The degree to which this may be possible for such layered 2−2

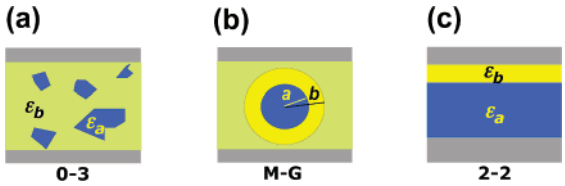

Figure 3. Dielectric structures analyzed in this study: (a) heterogeneous mixture of dielectric components (0−3 composite); (b) M−G spherical approximation where the ratio of the cubed radii (inclusion particle, sphere a, in total volume, sphere b) defines the volume fraction (f_a); (c) layers of two dielectric components (2−2 composite).

nanodielectrics (Figure 3c) is investigated herein. It will be shown that it is necessary to understand the effects of increased molecular permittivity on the total capacitance in order to estimate the highest capacitance achievable from SANDs.

The cross-linked polymer blend (CPB) has a completely different molecular arrangement (Figure 2b). These structures are fabricated by mixing and annealing either polystyrene (PS) or polyvinyl phenol (PVP) with α,ω-trichlorosilylalkane cross-linking reagents (e.g. $Cl_3Si(CH_2CH_2)_3SiCl_3$) to yield the dense blended structures CPS and CPVP, respectively.[4] The electrical properties of the resulting nanocomposites have also been characterized on a variety of substrates (n^+-Si, indium-tin-oxide, and Al) in MIS (metal−insulator−semiconductor) or MIM structures. The CPB nanodielectrics exhibit electrically uniform coverage over areas as large as 150 cm^2 and can be patterned with standard etching procedures. The dielectric properties of the MIS/MIM devices exhibit leakage current densities of 10^{-8} A/cm^2 and large capacitances ($\sim$300 nF/cm^2).[4] These materials are attractive for their solution-processability and compatibility with a wide range of substrates and semiconductors. However, to design other cross-linkable dielectrics with higher capacitances, one must first devise a model that describes the dielectric response of this type of nanocomposite.

The effective permittivity of two-phase composite dielectrics has been extensively studied using classical mixing rules such as the Polder−Van Santen (also called Bruggeman) and Maxwell−Garnett effective medium approximations (EMAs).[22−24] However, these models have not been applied to self-assembled and cross-linked polymeric thin films. For both types of nanoscopic dielectrics, the effective permittivity as a function of frequency is calculated here using the Maxwell−Wagner-modified Maxwell−Garnett model. The SAND nanodielectric is also considered here as two parallel plate capacitors in series, leading to important consequences that are discussed in the Results section. Despite the limitations of most EMAs, such as the requirement that the size of the inclusion must be smaller than the probing wavelength and that any interactions between the inclusion and matrix phases are negligible, these are common, experimentally verified methods for modeling mixed phases (0−3 composites; Figure 3a).[24−29] For example, Wong et al. found that the experimental permittivities of lead zirconate titanate−polyurethane 0−3 composites agree very well with the Bruggeman-computed effective permittivity.[30] Therefore, it is reasonable to apply EMAs to the present polymeric thin films in order to understand the observed capacitances and to develop means for predicting the capacitance characteristics of other nanodielectrics.

II. Theoretical Considerations

Classical mixing rules describe the effective permittivities of two-phase mixtures by volume averaging the two dielectric

permittivities.[31] The Maxwell−Garnett (M−G) formula

$$\epsilon_{\text{eff}} = \epsilon_{\text{b}} \frac{\epsilon_{\text{a}} + 2\epsilon_{\text{b}} + 2f_{\text{a}}(\epsilon_{\text{a}} - \epsilon_{\text{b}})}{\epsilon_{\text{a}} + 2\epsilon_{\text{b}} - f_{\text{a}}(\epsilon_{\text{a}} - \epsilon_{\text{b}})} \tag{2}$$

is derived based on the assumption that the field exciting the dispersed particles is simply a local field in homogeneously polarized matter. The entire mixture is modeled as an isotropic one-particle system (Figures 3a and b), where a spherical inclusion of permittivity ϵ_{a} is surrounded by a shell of insulating medium having a lower permittivity, ϵ_{b}. The volume fraction

$$f_{\text{a}} = \frac{a^3}{b^3} \tag{3}$$

is the ratio of the volume that the inclusion, sphere a, occupies within the total volume, sphere b (Figure 3b). The effective permittivity calculated for the single inclusion system is then assumed to be the effective permittivity of the bulk composite material, since any of the other inclusions could have been chosen and treated in the same way.

However, the M−G formula as written above is not valid for describing the frequency dependence of the effective permittivity. For the case of a heterogeneous dielectric where the inclusion phase, a, has a nonzero direct electrical conductivity, the Maxwell−Wagner theory[32,33] is used to modify the M−G formula to describe the corresponding low-frequency (<1 kHz) dielectric dispersion. This model uses the same M−G formula (eq 2) but replaces the permittivity of the dispersed material with its complex frequency-dependent permittivity, $\tilde{\eta}_{\text{a}}$, given by

$$\tilde{\eta}_{\text{a}} = \epsilon_{\text{a}} + \frac{4\pi\sigma_{\text{a}}}{i\omega} \tag{4}$$

where σ_{a} is the conductivity of the inclusion phase and ω is the angular frequency.[34] The real part of the effective permittivity can be written as

$$RE\epsilon_{\text{eff}}(\omega) = \epsilon_{\text{eff},\infty} + \frac{\epsilon_{\text{eff}}(0) - \epsilon_{\text{eff},\infty}}{1 + \omega^2\tau_{\text{eff}}^2} \tag{5}$$

where $\epsilon_{\text{eff},\infty}$ is given by eq 2, and $\epsilon_{\text{eff}}(0)$ is given by

$$\epsilon_{\text{eff}}(0) = \epsilon_{\text{b}}\left(1 + \frac{3f_{\text{a}}}{(1 - f_{\text{a}})}\right) \tag{6}$$

The relaxation time describing the charge accumulation that occurs at the particle−medium interface (τ_{eff}) is given by

$$\tau_{\text{eff}} = \frac{2\epsilon_{\text{b}} + \epsilon_{\text{a}} - f_{\text{a}}(\epsilon_{\text{a}} - \epsilon_{\text{b}})}{4\pi\sigma_{\text{a}}(1 - f_{\text{a}})} \tag{7}$$

Note that eq 6 results from the zero frequency limit of eq 5 for a conductive inclusion, and for the special case where $f_{\text{a}} = 1$ (only the inclusion material is present), the permittivity goes to infinity, as expected for a conductor.[33,34]

In real systems, the dispersed particles are not always perfect spheres. For a system with randomly oriented ellipsoidal inclusions, the Polder−Van Santen approximation

$$\epsilon_{\text{eff}} = \epsilon_{\text{b}} + \frac{f_{\text{a}}}{3}(\epsilon_{\text{a}} - \epsilon_{\text{b}}) \sum_{j=x,y,z} \frac{\epsilon_{\text{eff}}}{\epsilon_{\text{eff}} + N_j(\epsilon_{\text{a}} - \epsilon_{\text{eff}})} \tag{8}$$

can be used to calculate the effective permittivity.[22,23] This model is similar to that for the M−G approximation except that here the ellipsoidal shapes of the inclusions are taken into account by the depolarization factors, $N_{x,y,z}$. For needle-shaped prolate spheroids (one principal axis is much greater than the other), which is approximately the shape of the inclusions considered in this study, $N_x = 0$ and $N_y \approx N_z = 0.5$.[22] In this case, we can rewrite the Polder−Van Santen equation as

$$\epsilon_{\text{eff}} = \epsilon_{\text{b}} + \frac{f_{\text{a}}}{3}(\epsilon_{\text{a}} - \epsilon_{\text{b}})\left[1 + \frac{2\epsilon_{\text{eff}}}{\epsilon_{\text{eff}} + 0.5(\epsilon_{\text{a}} - \epsilon_{\text{eff}})}\right] \tag{9}$$

where the terms are the same as those in eq 2. Equation 9 is then solved for ϵ_{eff} in terms of ϵ_{a}, ϵ_{b}, and f_{a} using Maple (version 8.00). Again, this formula is derived with no frequency considerations and assumes static fields. To describe frequency-dependent data, eq 9 was treated in the same way as the M−G formula, where the particle permittivity (ϵ_{a}) was replaced with the complex frequency-dependent permittivity (eq 4). However, solving the frequency-dependent form of eq 9 for $\epsilon_{\text{eff}}(0)$ results in a singularity when $\omega = 0$, suggesting that the Polder−Van Santen formula is not valid in the low-frequency regime since we know experimentally that the dielectric does not behave as a metal at low frequency. Thus, the frequency dependence of both types of nanodielectrics is modeled here with only the modified M−G formula and not the modified Polder−Van Santen formula.

Since the components of the SAND are arranged in parallel layers, called a 2−2 composite (Figure 3c), modeling the effective permittivity of SANDs using the aforementioned EMAs may not be optimum. In addition to the frequency-dependent EMA model, the layered SAND nanodielectric is also viewed more simply and accurately using an equivalent circuit of two capacitors in series. To calculate the total capacitance, the permittivities of the two materials are summed according to

$$\frac{1}{C_{\text{tot}}} = \sum_i \frac{d_i}{\epsilon_i\epsilon_0} \tag{10}$$

In the present study, we use the two-capacitors-in-series equation to optimize and predict the capacitances of self-assembled nanodielectrics.

III. Results and Discussion

A. SAND Nanocomposite. The measured SAND capacitance has a moderate dependence on the frequency of the applied field (Figure 4a). The capacitance decays as the frequency increases, suggesting a well-characterized dielectric dispersion attributable to interfacial polarization effects between the two layers of differing permittivities and conductivities.[31] The approximate conductivity of the Stilbazolium (Stb) molecule ($\sigma_{\text{a}} = 2.3 \times 10^{-11}$ S/cm) is estimated from the leakage current density at 1.0 V for a n^+-Si/Stb/Au MIS device (assuming the film is pinhole-free). Using this value for the conductivity in eq 7, the calculated capacitance as a function of frequency (using eq 5) predicts a constant capacitance over the measured frequency range (Figure 4a). The magnitude of the computed capacitance (~1700 nF/cm^2) agrees well with the measured range of 2400−1500 nF/cm^2, which demonstrates the qualitative predictive power of the effective medium. However, the observed dielectric dispersion occurs at higher frequencies than those predicted by M−G, and the computed capacitance is smaller than the measured capacitance at 1000 Hz. Based on the results of this

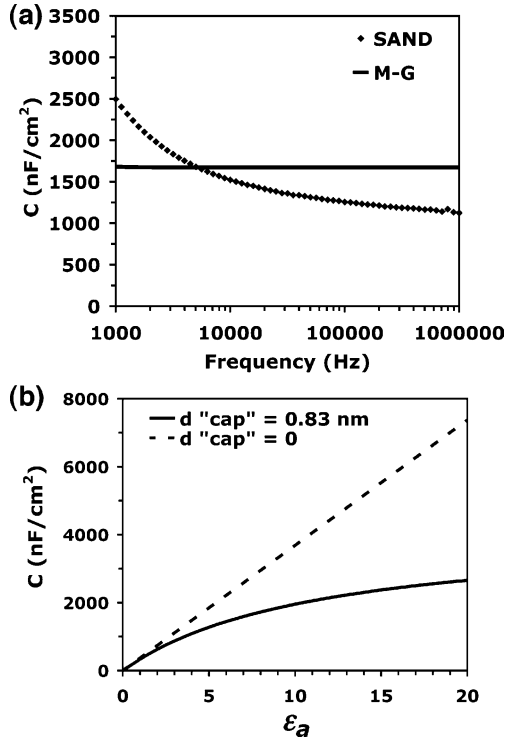

Figure 4. (a) Measured Stb-based SAND capacitance vs frequency data[3] compared to the frequency-dependent M−G-computed capacitance where the input parameters established by experiment are as follows: $d = 3.2$ nm, $f_a = 0.74$, $\sigma_a = 2.3 \times 10^{-11}$ S/cm, and $\epsilon_a = 7$ (back-calculated from high-frequency data).[3] (b) Two-capacitors-in-series-computed SAND capacitances vs the permittivity of the molecular layer with two different capping layer thicknesses (0 and 0.83 nm). Here, the input parameters established by experiment are as follows: $\epsilon_b = 3.9$, $d_b = 0.83$ nm, and $d_a = 2.4$ nm.[3]

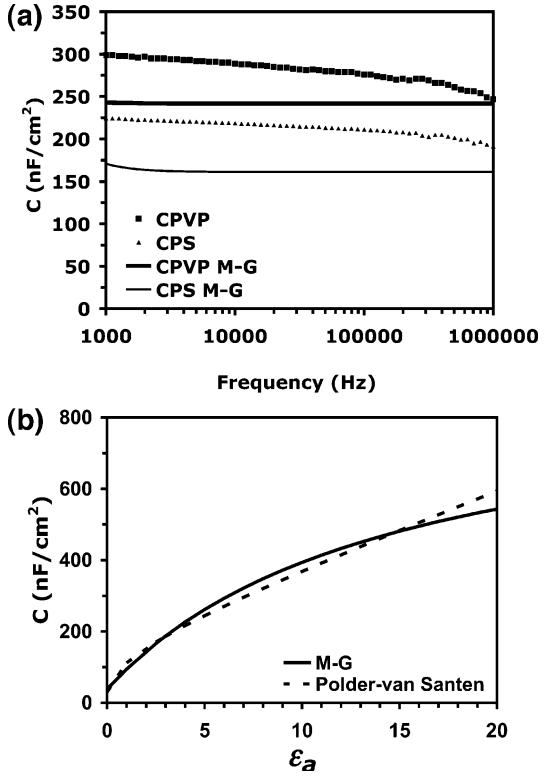

Figure 5. (a) Experimental capacitance vs frequency data for two CPB materials[4] compared to the frequency-dependent M−G-calculated capacitance. (b) Polder−Van Santen and M−G effective medium predictions for larger permittivity polymer inclusions. Input parameters as established by experiment are as follows: $d \sim 14$ nm, $\epsilon_b = 2.6$, $f_a = 0.50$, $\sigma_{PVP} = 3.34 \times 10^{-11}$ S/cm, and $\sigma_{PS} = 1.67 \times 10^{-11}$ S/cm.[4]

calculation, it is unclear if the observed low-frequency dispersion is due purely to interfacial polarization or other polarization mechanisms. A possible contributor is the oscillation of the I^- counterion with the alternating current (ac) field, which could lead to larger permittivities at low frequencies but is expected to decline by ~1 kHz, where ionic oscillations typically fall off.[22,35,36] Note, however, that the M−G approximation is not the most appropriate model to apply to 2−2 self-assembled thin films because of the underlying assumption that the composite is isotropic with randomly oriented inclusions, and the discrepancy between the theory and experiment may reflect the inadequacy of the model used.[37]

Because of the ordered structure of the self-assembled films, we employed an equivalent circuit of two capacitors in series to make predictions about future SANDs. The computed capacitance as a function of increasing π-molecular layer permittivity, ϵ_a, is plotted in Figure 4b. From this plot, it is possible to back-calculate the permittivity of the Stb molecule using the measured capacitance values at 10^3 and 10^6 Hz, respectively. We estimate the low-frequency limit permittivity to be ~16 and the high-frequency limit permittivity to be ~7. More importantly, increasing the permittivity of the molecular layer does not result in a continuing increase in capacitance, as shown in Figure 4b. Rather, the capacitance begins to plateau at ~3000 nF/cm^2 at an $\epsilon_a > 20$ (Figure 4b). This saturation behavior is a consequence of the two-capacitors-in-series model, where the total capacitance is limited by the lower permittivity material, which, in this case, is the capping layer (eq 10). The simplest strategy for an increase in capacitance would be to replace the capping layer with a high-permittivity material or to decrease the thickness by removing it altogether. The computed capacitance after deleting the capping layer is also plotted in Figure 4b. For this hypothetical nanodielectric, at $\epsilon_a = 16$, the maximum achievable capacitance is computed to be 5900 nF/cm^2. While this is a remarkably large capacitance, the leakage current properties of such hypothetical structures are at present unknown.

B. CPB Nanocomposites. Given the constraints of the layered 2−2 composite geometry, we investigated the ability of 0−3 CPB composites to achieve high capacitances. First, we determined if effective medium approximations can reproduce the experimental capacitance values, and then we made predictions using the EMAs for higher permittivity polymers. The experimental capacitances of the polymer blend composites are essentially constant within the measured frequency range up to 1 MHz (Figure 5a). The conductivities of PS ($\sigma_a = 1.67 \times 10^{-11}$ S/cm) and PVP ($\sigma_a = 3.34 \times 10^{-11}$ S/cm) were roughly estimated from the previously reported leakage current densities of MIS devices (n^+-Si/PS or PVP/Au) at 3 MV/cm[4,38] and were then used in the frequency-dependent M−G formula (eq 5). The computed M−G capacitances are also nonvarying over the frequency range shown. The calculated capacitances for CPVP ($C = 280$ nF/cm^2) and the CPS ($C = 150$ nF/cm^2) composites are in favorable agreement with the measured capacitance values[4] of 300 and 220 nF/cm^2 at 1 kHz. It is unclear if the deviations from the experimental data are due to the spherical approximation underlying the M−G theory or due to other neglected molecular-level details. Nonetheless, the theory seems able to predict the approximate value of the effective 1 kHz capacitance to within ~30%.

Since the EMA models seem adequate for a first approximation of the dielectric response in cross-linked polymeric materials, we use the M−G and Polder−Van Santen approximations

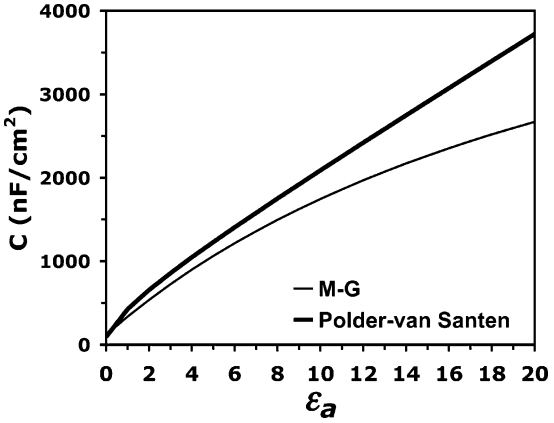

Figure 6. M−G- and Polder−Van Santen-derived capacitances for a hypothetical ultrathin CPB nanocomposite. Input parameters: $f_a = 0.74$ and $d = 3.2$ nm.

(staying in the high-frequency limit) to optimize the dielectric structure and to predict the capacitance of higher permittivity materials. The two approximations predict relatively similar capacitances for small permittivities, such as the cases of PVP ($\epsilon_a = 5$) and PS ($\epsilon_a = 2.5$), as shown in Figure 5b. However, as the polymer inclusion permittivity is raised to above ~20, the ellipsoidal (Polder−Van Santen) approximation begins to steadily increase above the M−G approximation, which begins to plateau to a lower capacitance. Therefore, according to the trends predicted by the Polder−Van Santen description, polymers with larger permittivities, such as PVA ($\epsilon_r = 7-10$)[11] or cyano-ethylpullulan ($\epsilon_r = 18.5$),[11] could be used profitably in place of PVP to enhance the dielectric properties of the blend for use as an OFET gate dielectric.

It may appear at first that the SAND structure is more desirable as a gate dielectric than the CPBs due to the larger capacitances. However, the measured thickness of the CPB nanocomposites is somewhat greater than that of the Stb-based SAND nanodielectric, which partly explains the lower capacitance. To compare the effect of the different geometries, a hypothetical thickness of 3.2 nm (d of SAND) was used to calculate the capacitance of the hypothetical CPBs (Figure 6). The Polder−Van Santen and M−G-computed capacitances (for this ultrathin CPB) at $\epsilon_a = 7$ are 1600 and 1400 nF/cm^2, respectively. These values are very close to the measured high-frequency capacitance of 1400 nF/cm^2 for the Stb-based 2−2 SAND nanodielectric. Based on this comparison, the two molecular arrangements will have essentially the same dielectric response for materials having smaller permittivities, but the 0−3 type of composite has the potential to afford larger capacitances as the permittivity of the polymeric inclusion is increased to above 18 (see Figure 6). Thus, future hybrid composites with nonspherical inclusions and large permittivities, such as metallic or high-ϵ_r perovskite nanoparticles, are attractive. This would permit the use of a realistic film thickness of 14 nm for cross-linked films, while exceeding the capacitances of the current materials. However, for these hybrid nanocomposites, a new method of calculating effective permittivities is required as effective medium approximations are less reliable when the components have very different permittivities.[39] Furthermore, new computational methods should include a better description of inclusion−matrix and matrix−matrix interactions as well as a self-consistent treatment of the electrostatics.[40]

IV. Conclusions

The effective permittivities of solution-processable SAND and CPB organic nanodielectrics have been investigated using EMA models. The agreement between calculated and measured capacitances shows that these methods provide a semiquantitative prediction and understanding of the permittivities and resulting capacitances of these nanodielectrics. The M−G frequency-dependent capacitance is within the range of the measured Stb-based SAND capacitance but underestimates the large measured capacitance at 1 kHz. Thus, the low-frequency data are still not completely understood, and future work will focus on modeling ionic polarization, while also exploring more structurally valid models. The two-capacitors-in-series description of the self-assembled film reveals that capacitance increases and eventually plateaus as the π-molecular component polarizability and permittivity increase. Larger capacitances should, in principle, be obtainable from SAND composites consisting of only a single molecular π-electron layer (no capping layer). Therefore, the geometry of the two capacitors in series may not completely optimize composite capacitances.

Alternatively, cross-linked polymer blend nanocomposites, modeled here as 0−3 composites using the Polder−Van Santen and M−G EMAs, may offer larger capacitances. The calculated frequency-dependent M−G capacitance agrees well with the experimental data but is somewhat smaller over the entire frequency range. Again, the EMA seems able to qualitatively predict the dielectric function for this class of materials. Future studies will focus on 0−3 composite materials with unconventional inclusions having large permittivities and capacitances, while maintaining the attractions of low-cost solution processing and compatibility with flexible substrates and OFET organic semiconductors. It is important to note that the effective medium models give rough guidelines for the expected effective permittivity of a given nanocomposite; however, a complete understanding of the physics behind the response behavior of these systems will require models that include molecular-level details.

Acknowledgment. This research was supported by the ONR MURI Program (N00014-02-1-0909), the Northwestern University MRSEC (DMR-0076097-006), and DARPA/ARO (48639-EL). We thank Dr. Myung-Han Yoon for sharing experimental data and for helpful discussions.

References and Notes

(1) Fontaine, P.; Goguenheim, D.; Deresmes, D.; Vuillaume, D. *Appl. Phys. Lett.* **1993**, *62*, 2256.
(2) Halik, M.; Klauk, H.; Zschleschang, U.; Schmid, G.; Dehm, C.; Schutz, M.; Maisch, S.; Effenberger, F.; Brunnbauer, M.; Stellacci, F. *Nature* **2004**, *431*, 963.
(3) Yoon, M.-H.; Facchetti, A.; Marks, T. J. *Proc. Natl. Acad. Sci. U.S.A.* **2005**, *102*, 4678.
(4) Yoon, M.-H.; Yan, H.; Facchetti, A.; Marks, T. J. *J. Am. Chem. Soc.* **2005**, *127*, 10388.
(5) Chen, F.-C.; Chu, C.-W.; He, C.; Yang, Y.; Lin, J.-L. *Appl. Phys. Lett.* **2004**, *85*, 3295.
(6) Schroeder, R.; Majewski, L. A.; Grell, M. *Adv. Mater.* **2005**, *17*, 1535.
(7) Ju, S.; Lee, K.; Janes, D.; Yoon, M.-H.; Facchetti, A.; Marks, T. J. *Nano Lett.* **2005**, *5*, 2281.
(8) Hur, S.-H.; Yoon, M.-H.; Gaur, A.; Shim, M.; Facchetti, A.; Marks, T. J.; Rogers, J. *J. Am. Chem. Soc.* **2005**, *127*, 13808.
(9) Wang, L.; Yoon, M.-H.; Facchetti, A.; Marks, T. J. *Nat. Mater.*, in press.
(10) Dimitrakopoulos, C. D.; Kymissis, I.; Purushothaman, S.; Neumayer, D. A.; Duncombe, P. R.; Laibowitz, R. B. *Adv. Mater.* **1999**, *11*, 1372.
(11) Facchetti, A.; Yoon, M.-H.; Marks, T. J. *Adv. Mater.* **2005**, *17*, 1705.
(12) Cao, Y.; Irwin, P. C.; Younsi, K. *IEEE Trans. Dielectr. Electr. Insul.* **2004**, *11*, 797.
(13) Deman, A.-L.; Tardy, J. *Org. Electron.* **2005**, *6*, 78.
(14) Dimitrakopoulos, C. D.; Malenfront, P. R. L. *Adv. Mater.* **2002**, *14*, 99.
(15) Veres, J.; Ogier, S.; Lloyd, G. *Chem. Mater.* **2004**, *16*, 4353.

(16) Wilk, G. D.; Wallace, R. M.; Anthony, J. M. *J. Appl. Phys.* **2001**, *89*, 5243.
(17) For advances in dielectrics of conventional semiconductors, see: Chau, R. S. *Technology@Intel Magazine*, January 2004; and references therein.
(18) (a) Murugaraj, P.; Mainwaring, D.; Mora-Huertas, N. *J. Appl. Phys.* **2005**, *98*, 054304−1. (b) Halik, M.; Klauk, H.; Zschieschang, U.; Schmid, G.; Radlik, W.; Weber, W. *Adv. Mater*. **2002**, *14*, 1717.
(19) Choy, T. C. *Effective Medium Theory: Principles and Applications International Series of Monographs on Physics*; Clarendon Press: Oxford, 1999.
(20) Sihvola, A. H.; Kong, J. A. *IEEE Trans. Geosci. Rem. Sens.* **1988**, *26*, 420.
(21) Du, H.; Chen, H.; Gong, J.; Wang, T. G.; Sun, C.; Lee, S. W.; Wen, L. S. *Appl. Surf. Sci*. **2004**, *233*, 99.
(22) Sihvola, A. *Electromagnetic Mixing Formulas and Applications*; Institution of Electrical Engineers: London, 1999.
(23) Polder, D.; Van Santen, J. H. *Physica* **1946**, *12*, 257−271.
(24) Rao, Y.; Qu, J.; Marinis, T.; Wong, C. P. *IEEE Trans. Compon., Packag. Technol.* **2000**, *23*, 1521.
(25) Jylha, L.; Sihvola, A. H. *IEEE Trans. Geosci. Rem. Sens*. **2005**, *43*, 59.
(26) Tuncert, E.; Serdyuk, Y. V.; Gubanski, S. M. *ArXiv: cond-mat/0111254.*
(27) Sareni, B.; Krahenbul, L.; Beroual, A.; Brosseau, C. *J. Appl. Phys.* **1997**, *81*, 2375.
(28) Ang, C.; Yu, Z.; Guo, R.; Bhalla, A. S. *J. Appl. Phys*. **2003**, *93*, 3475.
(29) Vo, H. T.; Shi, F. G. *Microelectron. J.* **2002**, *22*, 409.
(30) Lam, K. S.; Wong, Y. W.; Tai, L. S.; Poon, Y. M.; Shin, F. G. *J. Appl. Phys*. **2004**, *96*, 3896.
(31) Sinha, D.; Pillai, P. K. C. *J. Mater. Sci. Lett.* **1989**, *8*, 673.
(32) Inoue, T.; Pethig, R.; Al-Meen, T. A. K.; Burt, J. P. H.; Price, J. A. *J. Electrost.* **1988**, *21*, 215.
(33) Hanai, T. *Kolloid-Z.* **1960**, *171*, 23.
(34) Bottcher, C. J. F.; Bordewijk, P. *Theory of Electric Polarization: Dielectrics in Time Dependent Fields*; Elsevier Scientific Publishing Company: Amsterdam, 1978; Vol. II.
(35) Arroyo, F. J.; Delgado, A. V.; Carrique, F.; Jimenez, M. L.; Bellini, T.; Mantegazza, F. *J. Chem. Phys.* **2002**, *116*, 10973.
(36) (a) Giustino, F.; Pasquarello, A. *Phys. Rev. B* **2005**, *71*, 144104. (b) Bekkali, A.-E.-H.; Thurzo, I.; Kampen, T. U.; Zahn, D. R. T. *Appl. Surf. Sci.* **2004**, *234*, 149.
(37) Cole, K. S.; Cole, R. H. *J. Chem. Phys*. **1941**, *9*, 341.
(38) Assuming no extrinsic doping processes and a pinhole-free film.
(39) Levy, O.; Stroud, D. *Phys. Rev. B* **1997**, *56*, 8035.
(40) Bergman, D. J.; Li, X.; Kim, K.; Stroud, D. *Proc. SPIE−Int. Soc. Opt. Eng.* **2005**, *5924*, 118.